


## Theoretical model for prediction of high-strength metallic glasses

Nicolas Argibay<sup>1,\*</sup> and Michael Chandross<sup>2,\*</sup>

<sup>1</sup>*Division of Materials Sciences and Engineering, Ames National Laboratory, Ames, Iowa 50011, USA*

<sup>2</sup>*Material, Physical, and Chemical Sciences Center, Sandia National Laboratories, Albuquerque, New Mexico 87123, USA*

 (Received 3 August 2022; revised 23 September 2022; accepted 6 October 2022; published 22 November 2022)

A method for predicting the ideal strength of metallic glasses based on materials properties—without fitting parameters—is presented, and its accuracy demonstrated for multiple alloys. The theoretical basis for these predictions is the stress-activated transformation of short-range ordered atomic structures into flowing amorphous interfaces with the properties of a supercooled liquid. Our theory for pure metals is extended through a regular solution model in which the enthalpy of fusion is mollified by approximate changes in coordination number between the solid and liquid phases. Additional parameters come from empirical material properties such as density, heat of fusion, and melting temperature.

DOI: [10.1103/PhysRevMaterials.6.115602](https://doi.org/10.1103/PhysRevMaterials.6.115602)

### I. INTRODUCTION

Since the first report of glass-forming alloys in 1960 by Klement *et al.* [1], much has been learned about their extraordinary mechanical properties [2] and unique processing requirements [3]. However, fundamental questions remain about the nature of their strength and deformation mechanisms. These materials exhibit high mechanical strength at temperatures below their glass transition, above which viscous and delocalized flow can readily occur and lead to rapid softening. At lower temperatures, defects like voids and pores can curtail their strength by promoting premature failure through crack formation and fracture, a phenomenon that is associated with limited ductility. When fracture is avoided, these alloys show a purely elastic mechanical response up to extremely high stresses, and plastic deformation that is localized to what are called shear transformation zones (STZs) [2]. Here, we link this onset of plastic deformation to structural characteristics and materials properties exclusively, without fitting parameters. The present approach builds upon seminal work by Argon [4] and Spaepen [5], who treated inhomogeneous flow in metallic glasses as an activated process. A limiting factor in their models was the inability to accurately define the activation volume for the transition from locked and disordered solid to flowing states. We present a different description of inhomogeneous flow activation that accurately predicts the temperature-dependent strength of amorphous alloys by defining the specific free energy for plasticity as a function of materials properties.

Metallic glasses have been shown to have both short- and medium-range order (SRO and MRO)—conventionally associated with interatomic distances less than 0.5 nm, and between 0.5 and 2.0 nm, respectively [6]—through x-ray and electron diffraction measurements [7–19]. A truly random structure should have properties similar to those of a viscous liquid, but the properties of metallic glasses (MGs) at temperatures below their glass transition show fundamental differences from the liquid state. The densities of MGs are only slightly lower than the corresponding crystalline configurations of the same alloys [20–22], and this implies both efficient packing and the existence of SRO/MRO [23,24]. While it was initially believed that amorphous solid metals possess a liquidlike random structure [1], calculations based on this underpredict the densities of MGs [25]. The efficient cluster-packing (ECP) model [23,26] established a framework for describing the structure of MGs that reconciles the seemingly contradictory combination of high density and efficient packing with the absence of long-range order. In the ECP model, the structure of metallic glasses is described as generally consisting of a face-centered cubic (fcc) close-packed lattice, but rather than having individual atoms at lattice points, the motif consists of multiatom clusters, with a larger solute atom surrounded by smaller solvent atoms [23–26]. The difference in atomic radii leads to an average bond density or coordination number (CN) that is typically higher than that in crystal lattices; CNs in MGs are in the range  $CN = 8–20$  [24], while the closest-packed ordered structures, fcc crystals, have  $CN = 12$ . As we discuss below, the higher CNs are an important factor for understanding the unusually high strength of metallic glasses.

\*These authors contributed equally to this work.

†Corresponding author: [nargibay@ameslab.gov](mailto:nargibay@ameslab.gov)

‡Corresponding author: [mechand@sandia.gov](mailto:mechand@sandia.gov)

*Published by the American Physical Society under the terms of the Creative Commons Attribution 4.0 International license. Further distribution of this work must maintain attribution to the author(s) and the published article's title, journal citation, and DOI.*

### II. THEORY, RESULTS, AND DISCUSSION

As in our previous work on pure metals [27], we start with the assumption that the strength of MGs is related to the energy required to transform the glass from an efficiently packed solid state of atomic clusters to a randomly packed,

liquidlike configuration. Specifically, we relate the strength of MGs to the stress required to activate inhomogeneous flow below the glass transition temperature ( $T_g$ ). This calculation requires only empirical material properties and a quantitative estimate of the (efficient) packing fraction of the material.

We base the activation of flow for glassy alloys on the free energy difference between short-range ordered solid and liquid (i.e., flowing) states,  $\Delta G_{\text{flow}} = \Delta G_{\text{ord}} - \Delta G_{\text{dis}}$ , where  $\Delta G_{\text{ord}}$  and  $\Delta G_{\text{dis}}$  are the energies of the ordered and disordered states, respectively. Similar to a regular solution model, the activation energy for flow is approximated as the value for an ideal solution with a correction based on the enthalpy of mixing,  $\Delta H_{\text{mix}}$ . The activation energy for the ideal mixture is a rule-of-mixtures combination of the pure elemental constituents. In Eq. (1) we show the free energy change for an ideal solution at a temperature,  $T$ , where for each elemental constituent  $i$  (1,2,3 ...),  $X_i$  is the atomic or molar fraction,  $T_{m,i}$  is melting temperature, and  $L_i$  is the heat of fusion.

$$\Delta G_{\text{flow,ideal}}(T) = \sum_{i=1,2,\dots}^N X_i L_i \left(1 - \frac{T}{T_{m,i}}\right). \quad (1)$$

The correction to this ideal mixture is then the difference in the heats of mixing of the ordered ( $\Delta H_{\text{mix,ord}}$ ) and disordered ( $\Delta H_{\text{mix,dis}}$ ) solutions, such that

$$\Delta G_{\text{flow}} = \Delta G_{\text{ord}} - \Delta G_{\text{dis}} = \Delta G_{\text{flow,ideal}} + (\Delta H_{\text{mix,ord}} - \Delta H_{\text{mix,dis}}). \quad (2)$$

We determine the mixing enthalpies using the method described in Takeuchi and Inoue [28] that is based on the work of Miedema and co-workers [29–31]. To calculate the difference in ordered and disordered mixing enthalpies, we first consider the quasichemical theory of solutions [32, pp. 236ff.], where the enthalpy of mixing is proportional to the coordination number of atoms. This implies that the enthalpies of mixing will be different in the ordered and disordered states, with the overall effect being a mollified  $\Delta H_{\text{mix}}$  because of the different coordination numbers between these states,  $z_{\text{ord}}$  and  $z_{\text{dis}}$ , respectively. We make the simplifying assumption that the regular solution model can be applied to both the glassy (clustered SRO) and random (disordered) states such that  $\Delta H_{\text{mix}}$  is exclusively a function of composition, with negligible difference in the frequency of bond type; i.e., for elements A and B the fraction of A-A, B-B, and A-B bonds remains about the same in both the ordered/glassy and disordered/flowing states. This is not strictly true, and results in an underprediction of the impact of  $\Delta H_{\text{mix}}$  on strength, as the number of unlike bonds is higher in cluster-based SRO glasses. However, this allows for the tractable simplification that  $\Delta H_{\text{mix}}$  can be written as a function of a constant  $C$ , based on constituent bond energies, multiplied by the corresponding coordination number in each state. Assuming the bond energies are the same in the two states,  $\Delta H_{\text{mix,ord}} = z_{\text{ord}}C$  and  $\Delta H_{\text{mix,dis}} = z_{\text{dis}}C$ . Then, noting that  $\Delta H_{\text{mix,dis}} = \Delta H_{\text{mix}}$ , i.e., the mixing enthalpy from Takeuchi and Inoue [28] for a random solution, we arrive at a

final expression for  $\Delta G_{\text{flow}}$ ,

$$\Delta G_{\text{flow}} = \sum_{i=1,2,\dots}^N \left[ X_i L_i \left(1 - \frac{T}{T_{m,i}}\right) \right] + \left(1 - \frac{z_{\text{ord}}}{z_{\text{dis}}}\right) \Delta H_{\text{mix}}. \quad (3)$$

The use of a regular solution model implies that the entropies are similar for the glassy and flowing states. However, the ordered cluster cells will have inherently lower configurational entropy than a random close-packed or liquidlike mixture [32, pp. 240–243], so this approximation is not strictly correct. Despite this error, we show that strength predictions are still reasonably accurate.

As in our earlier work [27], the strength of metallic glasses is defined using an activated model for inhomogeneous flow where the strain rate is written as

$$\dot{\epsilon}_{\text{am}} = \dot{\epsilon}_{\text{tot}} \exp\left(-\frac{\Delta G_{\text{flow}} - \tau V^*}{k_B T}\right). \quad (4)$$

Here,  $\dot{\epsilon}_{\text{tot}}$  and  $\dot{\epsilon}_{\text{am}}$  correspond to the total applied strain rate and the strain rate transmitted to the flowing regions, respectively,  $k_B$  is the Boltzmann constant,  $\tau$  is the shear strength, and  $V^*$  is the activation volume. With MGs, unlike crystalline metals, intragranular deformation mechanisms are inactive and deformation is assumed to be limited to shear-activated flow via the formation of an amorphous or randomly packed interface. This is a possible explanation for the creation of STZs, which have been shown to have lower density than the parent material, i.e., closer to that of a liquid [33]. Thus, it is possible to make the simplifying assumption that  $\frac{\dot{\epsilon}_{\text{am}}}{\dot{\epsilon}_{\text{tot}}} \cong 1$ , as all plastic strain is accommodated by shear-activated flow, reducing Eq. (4) to the simple expression  $\tau(T) \cong \frac{\Delta G_{\text{flow}}(T)}{V^*}$ . For the rule-of-mixtures term we take the activation volume  $V^*$  for each elemental constituent to be the ratio of the corresponding elemental liquid density (at their melting temperature),  $\rho_i$ , and molar mass,  $M_i$ ; for the mixture term, it is similarly the ratio of alloy density,  $\rho_{\text{mix}}$ , and molar mass,  $M_{\text{mix}}$ ; i.e.,  $V_i^* = \frac{M_i}{\rho_i}$  and  $V_{\text{mix}}^* = \frac{M_{\text{mix}}}{\rho_{\text{mix}}}$ . Earlier work on the strength of crystalline metals [27] required a value for grain size in the strength calculation. For metallic glasses, we replace grain size with cluster cell size,  $d_{\text{cell}}$ , which can be approximated as having a consistent value of about 2 nm, explained in detail below. Combining expressions, we arrive at a complete expression for the shear stress required to activate flow,

$$\tau(T) = \sum_{i=1,2,\dots}^N \left[ X_i \left(L_i \frac{\rho_i}{M_i}\right) \left(1 - \frac{T}{T_{m,i}}\right) \left(\frac{d_{\text{cell}} - \delta_i}{d_{\text{cell}}}\right)^3 \right] + \left(\frac{z_{\text{dis}} - z_{\text{ord}}}{z_{\text{dis}}}\right) \left(\Delta H_{\text{mix}} \frac{\rho_{\text{mix}}}{M_{\text{mix}}}\right) \left(\frac{d_{\text{cell}} - \delta_{\text{mix}}}{d_{\text{cell}}}\right)^3. \quad (5)$$

This expression requires values for  $\delta_i$  and  $\delta_{\text{mix}}$ , the thickness of the amorphization or shear layer for elementally pure and alloyed systems, respectively. Both for pure metals and for alloys, glassy or ordered, the shear layer thickness is expected to be equivalent to the thickness of a high angle (low coordination) grain boundary, or approximately twice the size of the average atomic diameter, i.e.,  $\delta_i = 2d_i$  and  $\delta_{\text{mix}} = 2d_{\text{mix}}$  [27,34].

The atomic diameters,  $d_i$ , are taken from Pauling [35] for fully coordinated structures, and the average diameter of an

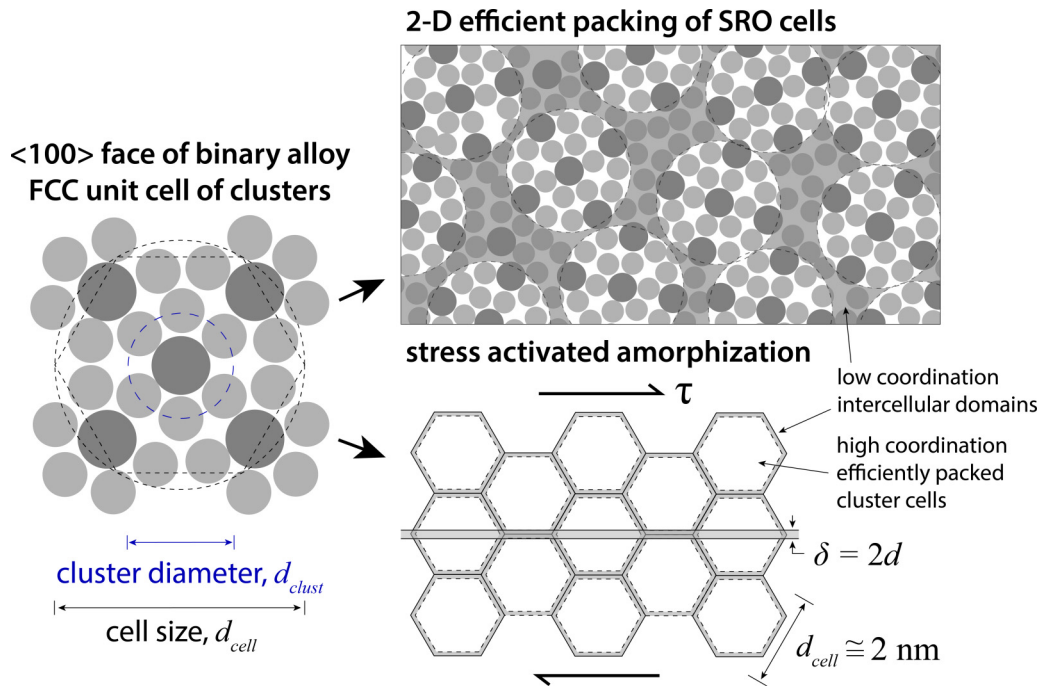


FIG. 1. Two-dimensional diagram of an efficiently packed clusters cell, how these can be packed with random orientations, and an idealized and annotated diagram of the parameters and length scales.

atom in a glassy alloy,  $d_{mix}$ , is calculated based on known alloy density and packing fraction following Eq. (6),

$$d_{mix} = 2 \left[ \frac{3}{4\pi} \left( \frac{M_{mix} f_p}{\rho_{mix} N_{Av}} \right) \right]^{1/3}. \quad (6)$$

In the case where these are unknown, we estimate a value using a rule-of-mixtures for the fully coordinated constituent elements. In Eq. (6),  $f_p$  is the packing fraction, approximated as 0.74 for close-packed atom clusters [26], and  $N_{Av}$  is Avogadro's number, used to convert density from a molar to per atom basis.

As a substitute for grain size (in the similar calculations for polycrystalline metals), we consider the size and periodicity of ordered domains in the glass. The basis for this consideration is that shear-activated flow across a series of ordered domains only requires rearrangement of a fraction of atoms, those that are highly coordinated compared to a liquid or amorphous state. For polycrystalline pure metals, the reasoning was that disordered grain boundaries reduce the energy cost of activating flow. For metallic glasses, this calculation must similarly account for the space between cluster cells wherein atoms already have a near random coordination. In this case, the value for the “equivalent grain size” is approximated as the size of a close-packed fcc cluster unit cell.

The approximate size of a cluster can be estimated using a simple approach based on the dimensions of fully coordinated (crystalline) metal atoms. Pauling [35] provides values for these, with an average radius of  $r_{atom} = 164 \text{ pm}$ . The average radius of a cluster is then the sum of the radius of one solvent atom (at the cluster center) and the radius of one solute atom (which forms a shell surrounding the central, solute atom), so that  $r_{clust} \cong 2r_{atom} = 328 \text{ pm}$ . The approximate diameter of a cluster  $d_{clust} = 656 \text{ pm}$ , which is also the separation between

close-packed clusters, agrees with the estimated value from high-resolution electron diffraction experiments for a binary  $\text{Cu}_{64}\text{Zr}_{36}$  metallic glass of  $\sim 0.6 \text{ nm}$  [19]. As illustrated in Fig. 1, metallic glasses consist of unit cells of efficiently packed clusters that tend towards fcc packing [24,26], with an approximate cluster lattice parameter,  $a_{clust} = \sqrt{2}d_{clust} = \sqrt{2}(656 \text{ pm}) \cong 928 \text{ pm}$ . This average value for the cluster cell lattice parameter is close to that from more complicated calculations that estimated the lattice parameter for 200 bulk metallic glass alloys to be  $980 \pm 133 \text{ pm}$  [26]. The unit cells are themselves randomly oriented, disrupting long-range order [23]. We must consider the cell size (i.e., equivalent grain size) for metallic glasses to be between the two-dimensional and three-dimensional packing of randomly oriented cubic unit cells, with a lower bound of slightly offset cubic cells,  $d_{cell,min} = \sqrt{3}a_{clust} \cong 1.6 \text{ nm}$ , and an upper bound of the diagonal distance of the fcc cell,  $d_{cell,max} = \sqrt{3}a_{clust} + d_{clust} \cong 2.2 \text{ nm}$ . This range agrees with measured crystallite sizes for Cu-Zr alloys that exhibited a transition to glassy behavior for grain sizes in the range 1–3 nm [36]. While more accurate estimates (with more accurate accounting of alloying effects) may improve the accuracy of predictions, the average value of  $d_{cell} \cong 2 \text{ nm}$  produces generally accurate results. These approximations also ignore factors that can be non-negligible [26], including the effects of coordination number on atom size.

Equation (5) also requires values for the coordination numbers of both the short-range ordered ( $z_{ord}$ ) and random-packed/liquidlike ( $z_{dis}$ ) states. For the disordered state, we use the average coordination number for pure liquid metals near their melting temperature,  $10.5 \pm 1.2$  [37,38]. The coordination number of efficiently packed atom cluster cells is more difficult to accurately determine. Analytic models,

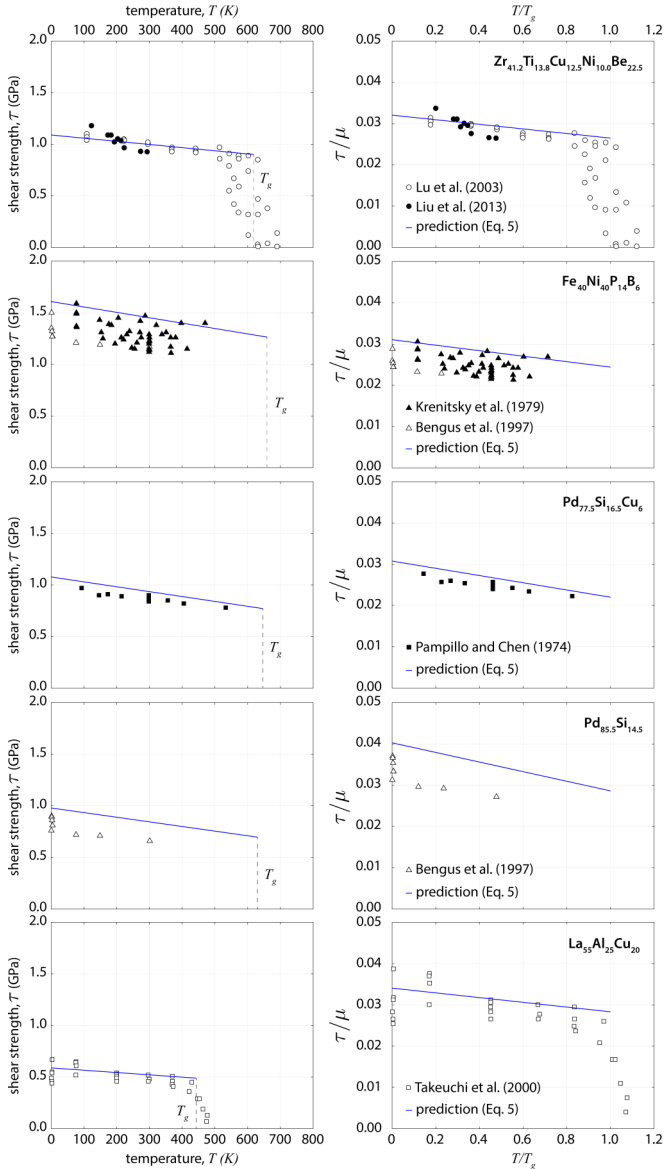


FIG. 2. (Left column) Survey of temperature-dependent shear strengths for multiple metallic glasses (sources: [43–49]) and (right column) with shear strengths normalized by room-temperature shear moduli and temperature normalized by corresponding glass transition temperatures;  $\mu$  is the room-temperature shear modulus.

like the efficient cluster-packing model, have been used to describe the structure and properties (including coordination number) of binary alloys [26]. However, values for ternary and higher-order alloys, which constitute the majority of experimental data on MGs, have so far only been tractable using computational methods such as molecular dynamics and *ab initio* simulations [36,39,40]. A method for calculating the coordination number for binary solvent-solute atom clusters ( $z_{clust,ij}$ ) based on the ratio ( $R_{ij}$ ) of atomic radii, was proposed by Egami [41] and later refined by Miracle *et al.* [42],

$$z_{clust,ij} = \frac{4\pi(1 - \frac{\sqrt{3}}{2})(R_{ij} + 1)}{1 - \sqrt{R_{ij}(R_{ij} + 2)}}. \quad (7)$$

Similarly, we estimate the average coordination number for the efficiently packed atomic cluster cells, corresponding

to the SRO/MRO solid state ( $z_{ord}$ ), using a compositionally weighted average of the binary elemental pairs,

$$z_{ord} = \sum_{i \neq j} (x_i + x_j) z_{c,i-j}. \quad (8)$$

All necessary parameters are shown in Table I, including the calculated coordination numbers. The estimated coordination numbers agree well for the few instances where values were available; for example, pairwise-correlation functions and Voronoi tessellation were used to determine the coordination number distribution for  $Zr_{41.2}Ti_{13.8}Cu_{12.5}Ni_{10}Be_{22.5}$  (vitreloy 1) [39], with an average value  $z_{ord} \cong 15$  that is comparable to the value  $z \cong 15.8$  from Eqs. (7) and (8).

We now compare temperature-dependent flow strength predictions from Eq. (5) to measured values for multiple metallic glasses in Fig. 2, both in absolute and normalized form, and find good agreement for alloys that exhibit a range of strengths and glass transition temperatures. In all cases, the predicted temperature dependence is accurate, and we note that the temperature dependence is fully defined by the rule-of-mixtures component in the activation energy (i.e., there is no temperature dependence in the mixing terms).

In Fig. 3(a), we show the correlation between room-temperature shear strengths and shear moduli, established by Johnson and Samwer [50]. Overlaid on this is a comparison with the rule-of-mixtures energy density ( $J/m^3$ ) from Eq. (1) normalized by the elemental atomic activation volumes. In this figure we have excluded the carbon-rich alloys from Johnson and Samwer [50] as the heat of fusion and melting temperature for nonmetals like carbon require additional considerations that are beyond the scope of this work.

Calculated room-temperature strengths with the regular solution model (for the metallic glasses listed in Table I) are compared to measured values in Fig. 3(b). Although there is good agreement, we note that there are multiple reasons why the measured strengths could be different than those predicted. Notably, the presence of defects that lead to crack initiation would result in strengths lower than those predicted. This is evident in the large spread in reported failure strengths in Fig. 2. An underestimation of coordination number, as would occur with partial crystallinity, would also result in a strength underprediction. For example, Choi-Yim *et al.* [52] reported about 2% crystalline phases in experiments with Ni-Nb-Sn, and these values correspond to the points with the largest prediction error (with measured strengths 2.0–2.3 GPa) in Fig. 1(b).

Given the good agreement with the geometry-independent energy density [Fig. 3(a)], the accurate prediction of temperature-dependent strength serves as a *post facto* justification of the assumptions about the ordered cell size, which is the parameter with the highest probable error. These results also suggest that, when structural disorder is properly characterized, the limiting strength of alloys can be generally predicted by elemental properties and mixing enthalpies. While we have previously shown that the strength of some dilute binary alloys (i.e., Ni-W [27] and Sm-Co [53]) can be accurately predicted using the ideal solution approach, it remains to be seen whether these ideas can be practically extended to alloys with higher chemical complexity, such as

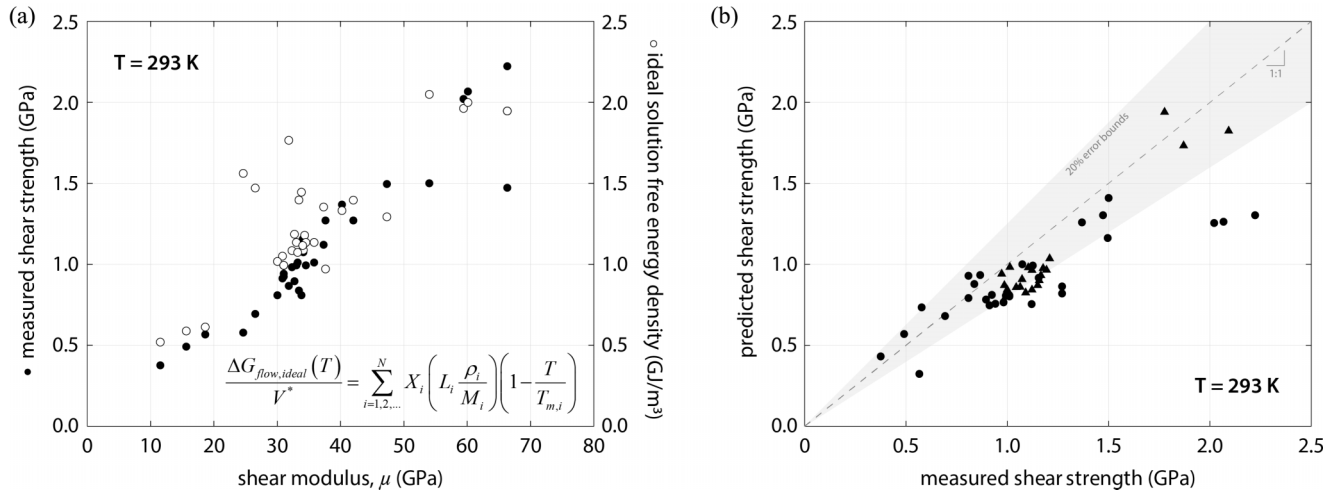


FIG. 3. (a) Comparison of measured strengths and free energy density as a function of shear modulus for metallic glass data from Johnson and Samwer (circles) [50], and (b) comparison of measured and predicted strengths also including high-entropy metallic glasses from Chen *et al.* (triangles) [51].

TABLE I. Summary of measured and calculated properties for metallic glasses at room temperature.

| Alloy  | $\rho_{RT}$<br>(g/cm <sup>3</sup> ) | $\mu_{RT}$<br>(GPa) | $T_g$<br>(K) | $M$<br>(kg/mol) | $H_{mix}^a$<br>(kJ/mol) | $z_{ord}$<br>(-) | $\tau_{Y,meas}$<br>(GPa) | $\tau_{Y,Eq.(5)}$<br>(GPa) | Error<br>(%) | Refs.      |
|--|-------------------------------------|---------------------|--------------|-----------------|-------------------------|------------------|--------------------------|----------------------------|--------------|------------|
| Zr <sub>41.2</sub> Ti <sub>13.8</sub> Cu <sub>12.5</sub> Ni <sub>10.0</sub> Be <sub>22.5</sub> | 5.9                                 | 34                  | 618          | 0.060           | -32.9                   | 15.8             | 1.07                     | 0.87                       | 19           | [43,59,60] |
| Zr <sub>48</sub> Nb <sub>8</sub> Ni <sub>12</sub> Cu <sub>14</sub> Be <sub>18</sub>            | 6.7                                 | 34                  | 620          | 0.069           | -31.1                   | 15.8             | 1.13                     | 0.88                       | 22           | [60]       |
| Zr <sub>55</sub> Ti <sub>5</sub> Cu <sub>20</sub> Ni <sub>10</sub> Al <sub>10</sub>            | 6.6                                 | 31                  | 625          | 0.074           | -30.9                   | 14.9             | 0.94                     | 0.65                       | 31           | [60]       |
| Zr <sub>57.5</sub> Nb <sub>5</sub> Cu <sub>15.4</sub> Ni <sub>12</sub> Al <sub>10</sub>        | 6.5                                 | 31                  | 663          | 0.077           | -30.8                   | 14.9             | 0.91                     | 0.64                       | 30           | [60]       |
| Zr <sub>55</sub> Al <sub>19</sub> Co <sub>19</sub> Cu <sub>7</sub>                             | 6.2                                 | 38                  | 733          | 0.071           | -39.1                   | 15.1             | 1.27                     | 0.83                       | 35           | [50]       |
| Pd <sub>40</sub> Cu <sub>30</sub> Ni <sub>10</sub> P <sub>20</sub>                             | 9.3                                 | 35                  | 593          | 0.074           | -26.8                   | 13.3             | 0.99                     | 0.92                       | 8            | [61]       |
| Pd <sub>40</sub> Cu <sub>30</sub> Ni <sub>10</sub> P <sub>20</sub>                             | 9.3                                 | 33                  | 593          | 0.074           | -26.8                   | 13.3             | 0.99                     | 0.92                       | 8            | [62]       |
| Pd <sub>40</sub> Cu <sub>30</sub> Ni <sub>10</sub> P <sub>20</sub>                             | 9.3                                 | 36                  | 595          | 0.074           | -26.8                   | 13.3             | 1.01                     | 0.92                       | 9            | [61]       |
| Pd <sub>60</sub> Cu <sub>20</sub> P <sub>20</sub>  | 9.8                                 | 32                  | 604          | 0.083           | -27.9                   | 13.4             | 0.98                     | 0.85                       | 13           | [60]       |
| Pd <sub>40</sub> Cu <sub>40</sub> P <sub>20</sub>  | 9.3                                 | 33                  | 548          | 0.074           | -29.2                   | 13.3             | 1.01                     | 0.93                       | 8            | [60]       |
| Ni <sub>45</sub> Ti <sub>20</sub> Zr <sub>25</sub> Al <sub>10</sub>                            | 6.4                                 | 40                  | 791          | 0.062           | -46.8                   | 14.9             | 1.37                     | 1.09                       | 20           | [63]       |
| Ni <sub>40</sub> Ti <sub>17</sub> Zr <sub>28</sub> Al <sub>10</sub> Cu <sub>5</sub>            | 6.5                                 | 47                  | 862          | 0.063           | -44.0                   | 14.7             | 1.50                     | 1.00                       | 33           | [63]       |
| Ni <sub>60</sub> Nb <sub>40</sub>  | 9.0                                 | 54                  | 885          | 0.073           | -29.4                   | 15.0             | 1.50                     | 1.36                       | 9            | [64,65]    |
| Ni <sub>60</sub> Nb <sub>35</sub> Sn <sub>5</sub>  | 8.6                                 | 66                  | 885          | 0.074           | -26.6                   | 15.2             | 2.22                     | 1.28                       | 42           | [52]       |
| Ni <sub>60</sub> Nb <sub>35</sub> Sn <sub>5</sub>  | 8.6                                 | 66                  | 885          | 0.074           | -26.6                   | 15.2             | 1.47                     | 1.28                       | 13           | [52]       |
| Ni <sub>60</sub> Sn <sub>6</sub> Nb <sub>27.2</sub> Ta <sub>6.8</sub>                          | 9.2                                 | 59                  | 875          | 0.080           | -26.5                   | 14.8             | 2.02                     | 1.24                       | 39           | [50]       |
| Ni <sub>60</sub> Sn <sub>6</sub> Nb <sub>20.4</sub> Ta <sub>13.6</sub>                         | 9.8                                 | 60                  | 882          | 0.086           | -26.7                   | 14.8             | 2.07                     | 1.25                       | 40           | [50]       |
| Cu <sub>64</sub> Zr <sub>36</sub>  | 8.1                                 | 34                  | 787          | 0.074           | -21.9                   | 16.2             | 1.15                     | 0.74                       | 36           | [66]       |
| Cu <sub>46</sub> Zr <sub>54</sub>  | 7.6                                 | 30                  | 696          | 0.079           | -22.2                   | 16.2             | 0.81                     | 0.64                       | 21           | [67]       |
| Cu <sub>46</sub> Zr <sub>42</sub> Al <sub>7</sub> Y <sub>5</sub>                               | 7.2                                 | 31                  | 713          | 0.074           | -25.8                   | 15.6             | 0.92                     | 0.70                       | 25           | [68]       |
| Pd <sub>77.5</sub> Si <sub>16.5</sub> Cu <sub>6.0</sub>  | 10.4                                | 35                  | 550          | 0.091           | -21.4                   | 13.3             | 0.87                     | 0.92                       | -7           | [69]       |
| Pt <sub>60</sub> Ni <sub>15</sub> P <sub>25</sub>  | 15.7                                | 34                  | 488          | 0.134           | -27.2                   | 13.7             | 0.81                     | 1.00                       | -23          | [70]       |
| Pt <sub>57.5</sub> Cu <sub>14.7</sub> Ni <sub>5</sub> P <sub>22.8</sub>                        | 15.2                                | 33                  | 490          | 0.132           | -27.0                   | 13.5             | 0.84                     | 0.95                       | -14          | [71,72]    |
| Pd <sub>64</sub> Ni <sub>16</sub> P <sub>20</sub>  | 10.1                                | 33                  | 452          | 0.084           | -23.1                   | 13.6             | 0.89                     | 0.85                       | 5            | [69]       |
| Mg <sub>65</sub> Cu <sub>25</sub> Gd <sub>10</sub>   | 4.0                                 | 19                  | 428          | 0.047           | -6.8                    | 16.0             | 0.57                     | 0.30                       | 47           | [50]       |
| La <sub>55</sub> Al <sub>25</sub> Cu <sub>10</sub> Ni <sub>5</sub> Co <sub>5</sub>             | 6.0                                 | 16                  | 430          | 0.095           | -29.4                   | 17.4             | 0.49                     | 0.52                       | -6           | [60,73]    |
| Ce <sub>70</sub> Al <sub>10</sub> Ni <sub>10</sub> Cu <sub>10</sub>                            | 6.7                                 | 12                  | 359          | 0.113           | -21.7                   | 17.4             | 0.38                     | 0.36                       | 3            | [74]       |
| Cu <sub>50</sub> Hf <sub>43</sub> Al <sub>7</sub>  | 11.0                                | 42                  | 774          | 0.110           | -20.3                   | 15.0             | 1.27                     | 0.73                       | 43           | [50]       |
| Cu <sub>57.5</sub> Hf <sub>27.5</sub> Ti <sub>15</sub>   | 9.9                                 | 37                  | 729          | 0.093           | -14.6                   | 15.0             | 1.12                     | 0.67                       | 40           | [50]       |
| Au <sub>49.5</sub> Ag <sub>5.5</sub> Pd <sub>2.3</sub> Cu <sub>26.9</sub> Si <sub>16.3</sub>   | 11.6                                | 27                  | 405          | 0.128           | -11.7                   | 13.6             | 0.69                     | 0.68                       | 2            | [75]       |
| Au <sub>55</sub> Cu <sub>25</sub> Si <sub>20</sub>   | 12.2                                | 25                  | 348          | 0.130           | -11.9                   | 13.9             | 0.58                     | 0.73                       | -27          | [75]       |

<sup>a</sup>Heat of mixing determined using the method described in Takeuchi and Inoue [28], based on Boom, De Boer, and Miedema [29,30].

high-entropy or complex-concentrated alloys, which are solid solution crystalline compounds with high concentrations of multiple elements [54,55].

### III. SUMMARY AND CONCLUSIONS

Work by Inoue, Johnson, and others established alloy design criteria for metallic glasses. Building on this foundation, our work provides a means to predict which glasses are likely to be high strength. In this case, geometric considerations are likely unnecessary, as a simple calculation of the free energy of an ideal solution is sufficient. Combining this with computationally rapid assessments of ductility via the Pugh ratio (i.e., the ratio of shear and bulk moduli) [56,57], this work provides a framework for the discovery and optimization of metallic glasses.

It is likely that this framework can be extended to a broader set of alloys, including high-configurational entropy multi-principal-element alloys (solid solutions without a

majority elemental constituent) and intermetallic compounds (like those used to impart high strength and temperature resistance in superalloys [55,58]). The link between coordination number, formation free energy, and ultimate strength may reduce the computational cost in the search for thermally stable alloys with desirable mechanical properties.

### ACKNOWLEDGMENTS

This work was funded by the Laboratory Directed Research and Development program at Sandia National Laboratories, a multimission laboratory managed and operated by National Technology and Engineering Solutions of Sandia, LLC., a wholly owned subsidiary of Honeywell International, Inc., for the U.S. Department of Energy's National Nuclear Security Administration under Contract No. DE-NA0003525. Any subjective views or opinions that might be expressed in the paper do not necessarily represent the views of the U.S. Department of Energy or the United States Government.

- 
- [1] W. Klement, R. H. Willens, and P. O. L. Duwez, Non-crystalline structure in solidified gold–silicon alloys, *Nature (London)* **187**, 869 (1960).
  - [2] C. A. Schuh, T. C. Hufnagel, and U. Ramamurty, Mechanical behavior of amorphous alloys, *Acta Mater.* **55**, 4067 (2007).
  - [3] J. Schroers, Processing of bulk metallic glass, *Adv. Mater.* **22**, 1566 (2010).
  - [4] A. S. Argon, Plastic deformation in metallic glasses, *Acta Metall.* **27**, 47 (1979).
  - [5] F. Spaepen, A microscopic mechanism for steady state inhomogeneous flow in metallic glasses, *Acta Metall.* **25**, 407 (1977).
  - [6] T. C. Hufnagel and S. Brennan, Short- and medium-range order in  $(\text{Zr}_{70}\text{Cu}_{20}\text{Ni}_{10})_{90-x}\text{Ta}_x\text{Al}_{10}$  bulk amorphous alloys, *Phys. Rev. B* **67**, 014203 (2003).
  - [7] J. Sietsma and B. J. Thijsse, An investigation of universal medium range order in metallic glasses, *J. Non-Cryst. Solids* **135**, 146 (1991).
  - [8] L. Zhang, Y. Wu, X. Bian, H. Li, W. Wang, and S. Wu, Short-range and medium-range order in liquid and amorphous  $\text{Al}_{90}\text{Fe}_5\text{Ce}$  alloys, *J. NonCryst. Solids* **262**, 169 (2000).
  - [9] Y. Hirotsu, M. Matsushita, T. Ohkubo, A. Makino, and T. Oikawa, Average and local structures of amorphous  $\text{Pd}_{75}\text{Si}_{25}$  alloy analyzed by modern electron diffraction techniques, *Mater. Sci. Eng. A* **226-228**, 274 (1997).
  - [10] J.-M. Dubois, F. Montoya, and C. Back, Icosahedral order in glass-forming metallic melts, *Mater. Sci. Eng., A* **178**, 285 (1994).
  - [11] L. Červinka, Modeling of medium-range order in metallic glasses: calculation of x-ray scattering in a  $\text{Ti}_{61}\text{Cu}_{16}\text{Ni}$  glass, *J. Non-Cryst. Solids* **156-158**, 94 (1993).
  - [12] P. Lamparter, S. Steeb, and E. Grallath, Neutron diffraction study on the structure of the metallic glass  $\text{Cu}_{57}\text{Zr}_{43}$ , *Z. Naturforsch., A: Phys. Sci.* **38**, 1210 (1983).
  - [13] V. Petkov, A. Apostolov, and H. Sassik, Short-range order in  $\text{Gd}_4\text{Cu}_3$  metallic glass, *J. Non-Cryst. Solids* **122**, 262 (1990).
  - [14] L. Červinka, Medium-range ordering in non-crystalline solids, *J. Non-Cryst. Solids* **90**, 371 (1987).
  - [15] J. M. Dubois and G. Le Caer, Ordre local et proprietes physiques des verres metalliques riches en fer, *Acta Metall.* **32**, 2101 (1984).
  - [16] P. H. Gaskell, On the structure of simple inorganic amorphous solids, *J. Phys. C: Solid State Phys.* **12**, 4337 (1979).
  - [17] P. H. Gaskell, Models for the structure of amorphous metals, *Glassy Metal II*, Topics in Applied Physics 5 (Springer, New York, 1983), Vol. 53, p. 5.
  - [18] P. Lamparter, W. Sperl, and S. Steeb, Atomic structure of amorphous metallic  $\text{Ni}_{81}\text{B}_{19}$ , *Z. Naturforsch., A: Phys. Sci.* **37**, 1223 (1982).
  - [19] A. C. Y. Liu, M. J. Neish, G. Stokol, G. A. Buckley, L. A. Smillie, M. D. de Jonge, R. T. Ott, M. J. Kramer, and L. Bourgeois, Systematic Mapping of Icosahedral Short-Range Order in a Melt-Spun  $\text{Zr}_{36}\text{Cu}_{64}$  Metallic Glass, *Phys. Rev. Lett.* **110**, 205505 (2013).
  - [20] G. M. Dougherty, Y. He, G. J. Shiflet, and S. J. Poon, Compositional dependence of glass formability in Al-Ni-Fe-Gd amorphous alloys, *Scr. Metall. Mater.* **30**, 101 (1994).
  - [21] A. Inoue, High tensile strength bulk glassy alloy, *Mater. Sci. Eng., A* **267**, 171 (1999).
  - [22] A. R. Yavari, J.-L. Uriarte, and A. Inoue, Volume effects in amorphisation by rapid solidification and solid state reaction and in bulk glass-forming alloys, *Mater. Sci. Forum* **269-272**, 533 (1998).
  - [23] D. B. Miracle, A structural model for metallic glasses, *Nat. Mater.* **3**, 697 (2004).
  - [24] D. B. Miracle, The efficient cluster packing model—An atomic structural model for metallic glasses, *Acta Mater.* **54**, 4317 (2006).
  - [25] D. B. Miracle, Efficient local packing in metallic glasses, *J. Non-Cryst. Solids* **342**, 89 (2004).
  - [26] D. B. Miracle, The density and packing fraction of binary metallic glasses, *Acta Mater.* **61**, 3157 (2013).

- [27] M. Chandross and N. Argibay, Ultimate Strength of Metals, *Phys. Rev. Lett.* **124**, 125501 (2020).
- [28] A. Takeuchi and A. Inoue, Mixing enthalpy of liquid phase calculated by Miedema's scheme and approximated with sub-regular solution model for assessing forming ability of amorphous and glassy alloys, *Intermetallics* **18**, 1779 (2010).
- [29] R. Boom, F. R. De Boer, and A. R. Miedema, On the heat of mixing of liquid alloys—I, *J. Less-Common Met.* **45**, 237 (1976).
- [30] R. Boom, F. R. De Boer, and A. R. Miedema, On the heat of mixing of liquid alloys—II, *J. Less-Common Met.* **46**, 271 (1976).
- [31] A. R. Miedema, F. R. De Boer, and P. F. De Chatel, Empirical description of the role of electronegativity in alloy formation, *J. Phys. F: Met. Phys.* **3**, 1558 (1973).
- [32] R. DeHoff, *Thermodynamics in Materials Science* (CRC Press, Boca Raton, FL, 2006).
- [33] E. Bouchbinder, J. S. Langer, and I. Procaccia, Athermal shear-transformation-zone theory of amorphous plastic deformation. I. Basic principles, *Phys. Rev. E* **75**, 036107 (2007).
- [34] G. Gottstein and L. S. Shvindlerman, *Grain Boundary Migration in Metals: Thermodynamics, Kinetics, Applications*, 2nd ed. (CRC Press LLC, Baton Rouge, 2009).
- [35] L. Pauling, Atomic radii and interatomic distances in metals, *J. Am. Chem. Soc.* **69**, 542 (1947).
- [36] T. Brink and K. Albe, From metallic glasses to nanocrystals: Molecular dynamics simulations on the crossover from glass-like to grain-boundary-mediated deformation behaviour, *Acta Mater.* **156**, 205 (2018).
- [37] A. L. Hines, H. A. Walls, and K. R. Jethani, Determination of the coordination number of liquid metals near the melting point, *Metall. Trans. A* **16**, 267 (1985).
- [38] Y. Waseda, *Liquid Metals* (Institute of Physics, London, 1976).
- [39] C. Y. Lee, Z. H. Stachurski, and T. Richard Welberry, The geometry, topology and structure of amorphous solids, *Acta Mater.* **58**, 615 (2010).
- [40] J. Hafner, *ab-initio* simulations of materials using VASP: Density-functional theory and beyond, *J. Comput. Chem.* **29**, 2044 (2008).
- [41] T. Egami, Universal criterion for metallic glass formation, *Mater. Sci. Eng., A* **226-228**, 261 (1997).
- [42] D. B. Miracle, W. S. Sanders, and O. N. Senkov, The influence of efficient atomic packing on the constitution of metallic glasses, *Philos. Mag.* **83**, 2409 (2003).
- [43] J. Lu, G. Ravichandran, and W. L. Johnson, Deformation behavior of the  $Zr_{41.2}Ti_{13.8}Cu_{12.5}Ni_{10}Be_{22.5}$  bulk metallic glass over a wide range of strain-rates and temperatures, *Acta Mater.* **51**, 3429 (2003).
- [44] V. Z. Bengus, E. D. Tabachnikova, P. Duhaj, and V. Ocelík, Low temperature mechanical properties of metallic glasses connection with structure, *Mater. Sci. Eng., A* **226-228**, 823 (1997).
- [45] D. J. Krenitsky and D. G. Ast, Temperature dependence of the flow stress and ductility of annealed and unannealed amorphous  $Fe_{40}Ni_{40}P_{14}B_6$ , *J. Mater. Sci.* **14**, 275 (1979).
- [46] S. Takeuchi, T. Kakegawa, T. Hashimoto, A.-P. Tsai, and A. Inoue, Low temperature mechanical properties of bulk metallic glasses, *Mater. Trans. JIM* **41**, 1443 (2000).
- [47] A. Wisitsorasak and P. G. Wolynes, On the strength of glasses, *Proc. Natl. Acad. Sci. USA* **109**, 16068 (2012).
- [48] C. A. Pampillo and H. S. Chen, Comprehensive plastic deformation of a bulk metallic glass, *Mater. Sci. Eng.* **13**, 181 (1974).
- [49] Z. Y. Liu, G. Wang, K. C. Chan, J. L. Ren, Y. J. Huang, X. L. Bian, X. H. Xu, D. S. Zhang, Y. L. Gao, and Q. J. Zhai, Temperature dependent dynamics transition of intermittent plastic flow in a metallic glass. I. Experimental investigations, *J. Appl. Phys.* **114**, 033520 (2013).
- [50] W. L. Johnson and K. Samwer, A Universal Criterion for Plastic Yielding of Metallic Glasses with a  $(T/T_g)^{2/3}$  Temperature Dependence, *Phys. Rev. Lett.* **95**, 195501 (2005).
- [51] Y. Chen, Z.-W. Dai, and J.-Z. Jiang, High entropy metallic glasses: Glass formation, crystallization and properties, *J. Alloys Compd.* **866**, 158852 (2021).
- [52] H. Choi-Yim, D. Xu, and W. L. Johnson, Ni-based bulk metallic glass formation in the Ni-Nb-Sn and Ni-Nb-Sn-X ( $X = B, Fe, Cu$ ) alloy systems, *Appl. Phys. Lett.* **82**, 1030 (2003).
- [53] M. Chandross and N. Argibay, Friction of metals: A review of microstructural evolution and nanoscale phenomena in shearing contacts, *Tribol. Lett.* **69**, 119 (2021).
- [54] E. P. George, D. Raabe, and R. O. Ritchie, High-entropy alloys, *Nat. Rev. Mater.* **4**, 515 (2019).
- [55] D. B. Miracle and O. N. Senkov, A critical review of high entropy alloys and related concepts, *Acta Mater.* **122**, 448 (2017).
- [56] O. N. Senkov and D. B. Miracle, Generalization of intrinsic ductile-to-brittle criteria by Pugh and Pettifor for materials with a cubic crystal structure, *Sci. Rep.* **11**, 4531 (2021).
- [57] S. F. Pugh, XCII. Relations between the elastic moduli and the plastic properties of polycrystalline pure metals, *Philos. Mag. (1798-1977)* **45**, 823 (1954).
- [58] O. N. Senkov, D. B. Miracle, K. J. Chaput, and J. P. Couzinie, Development and exploration of refractory high entropy alloys—A review, *J. Mater. Res.* **33**, 3092 (2018).
- [59] F. Szuets, C. P. Kim, and W. L. Johnson, Mechanical properties of  $Zr_{56.2}Ti_{13.8}Nb_{5.0}Cu_{6.9}Ni_{5.6}Be_{12.5}$  ductile phase reinforced bulk metallic glass composite, *Acta Mater.* **49**, 1507 (2001).
- [60] W. H. Wang, C. Dong, and C. H. Shek, Bulk metallic glasses, *Mater. Sci. Eng.: R: Rep.* **44**, 45 (2004).
- [61] U. Harms, O. Jin, and R. B. Schwarz, Effects of plastic deformation on the elastic modulus and density of bulk amorphous  $Pd_{40}Ni_{10}Cu_{30}P_{20}$ , *J. Non-Cryst. Solids* **317**, 200 (2003).
- [62] N. Nishiyama, A. Inoue, and J. Z. Jiang, Elastic properties of  $Pd_{40}Cu_{30}Ni_{10}P_{20}$  bulk glass in supercooled liquid region, *Appl. Phys. Lett.* **78**, 1985 (2001).
- [63] D. Xu, G. Duan, W. L. Johnson, and C. Garland, Formation and properties of new Ni-based amorphous alloys with critical casting thickness up to 5 mm, *Acta Mater.* **52**, 3493 (2004).
- [64] L. Xia, W. H. Li, S. S. Fang, B. C. Wei, and Y. D. Dong, Binary Ni-Nb bulk metallic glasses, *J. Appl. Phys.* **99**, 026103 (2006).
- [65] Z. Zhu, H. Zhang, D. Pan, W. Sun, and Z. Hu, Fabrication of binary Ni-Nb bulk metallic glass with high strength and compressive plasticity, *Adv. Eng. Mater.* **8**, 953 (2006).
- [66] D. Xu, B. Lohwongwatana, G. Duan, W. L. Johnson, and C. Garland, Bulk metallic glass formation in binary Cu-rich alloy series— $Cu_{100-x}Zr_x$  ( $x = 34, 36, 38.2, 40$  at.%) and mechanical properties of bulk  $Cu_{64}Zr_{36}$  glass, *Acta Mater.* **52**, 2621 (2004).
- [67] G. Duan, D. Xu, Q. Zhang, G. Zhang, T. Cagin, W. L. Johnson, and W. A. Goddard, Molecular dynamics study of the binary  $Cu_{46}Zr_{54}$  metallic glass motivated by experiments: Glass formation and atomic-level structure, *Phys. Rev. B* **71**, 224208 (2005).

- [68] D. Xu, G. Duan, and W. L. Johnson, Unusual Glass-Forming Ability of Bulk Amorphous Alloys Based on Ordinary Metal Copper, *Phys. Rev. Lett.* **92**, 245504 (2004).
- [69] B. Golding, B. G. Bagley, and F. S. L. Hsu, Soft Transverse Phonons in a Metallic Glass, *Phys. Rev. Lett.* **29**, 68 (1972).
- [70] H. S. Chen, J. T. Krause, and E. Coleman, Elastic constants, hardness and their implications to flow properties of metallic glasses, *J. Non-Cryst. Solids* **18**, 157 (1975).
- [71] J. Schroers and W. L. Johnson, Ductile Bulk Metallic Glass, *Phys. Rev. Lett.* **93**, 255506 (2004).
- [72] J. Schroers and W. L. Johnson, Highly processable bulk metallic glass-forming alloys in the Pt–Co–Ni–Cu–P system, *Appl. Phys. Lett.* **84**, 3666 (2004).
- [73] Y. Zhang, D. Q. Zhao, R. J. Wang, and W. H. Wang, Formation and properties of  $Zr_{48}Nb_8Cu_{14}Ni_{12}Be_{18}$  bulk metallic glass, *Acta Mater.* **51**, 1971 (2003).
- [74] B. Zhang, M. X. Pan, D. Q. Zhao, and W. H. Wang, “Soft” bulk metallic glasses based on cerium, *Appl. Phys. Lett.* **85**, 61 (2004).
- [75] J. Schroers, B. Lohwongwatana, W. L. Johnson, and A. Peker, Gold based bulk metallic glass, *Appl. Phys. Lett.* **87**, 061912 (2005).